2011

Measurements of single top quark production cross sections and $|V_{tb}|$ in $p\bar{p}$ collisions at $\sqrt{s}$= 1.96 TeV

V. M. Abazov
Joint Institute for Nuclear Research, Dubna, Russia

Kenneth A. Bloom
University of Nebraska - Lincoln, kbloom2@unl.edu

Daniel R. Claes
University of Nebraska - Lincoln, dclaes@unl.edu

Kayle DeVaughan
University of Nebraska-Lincoln

Aaron Dominguez
University of Nebraska-Lincoln, aarond@unl.edu

See next page for additional authors

Measurements of single top quark production cross sections and $|V_{tb}|$ in $p\bar{p}$ collisions at $\sqrt{s} = 1.96$ TeV

V. M. Abazov,[34] B. Abbott,[72] B. S. Acharya,[28] M. Adams,[48] T. Adams,[46] G. D. Alexeev,[34] G. Alkhazov,[38] A. Alton,[60,*] G. Alverson,[59] G. A. Alves,[2] M. Aoki,[47] M. Arov,[57] A. Askew,[46] B. Åsman,[40] S. Atkins,[57] O. Atramentov,[64] K. Augsten,[9] C. Avila,[7] J. BackusMayes,[79] F. Badaud,[12] L. Bagby,[47] B. Baldin,[47] D. V. Bandurin,[46] S. Banerjee,[28] E. Barberis,[59] P. Baringer,[55] J. Barreto,[3] J. F. Bartlett,[47] U. Bassler,[17] V. Bazterra,[48] A. Bean,[55] M. Begalli,[3] M. Begel,[70] C. Belanger-Champagne,[40] L. Bellantoni,[47] S. B. Beri,[26] G. Bernardi,[16] R. Bernhard,[21] I. Bertram,[41] M. Besançon,[17] R. Beuselinck,[42] V. A. Bezzubov,[37] P. C. Bhat,[47] V. Bhatnagar,[26] G. Blazey,[49] S. Blessing,[46] K. Bloom,[63] A. Boehnlein,[47] D. Boline,[69] E. E. Boos,[36] G. Borissov,[41] T. Bose,[58] A. Brandt,[75] O. Brandt,[22] R. Brock,[61] G. Brooijmans,[67] A. Bross,[47] D. Brown,[16] J. Brown,[16] X. B. Bu,[47] M. Buehler,[47] V. Buescher,[23] V. Bunichev,[36] S. Burdin,[41,†] T. H. Burnett,[79] C. P. Buszello,[40] B. Calpas,[14] E. Camacho-Pérez,[31] M. A. Carrasco-Lizarraga,[55] B. C. K. Casey,[47] H. Castilla-Valdez,[31] S. Chakrabarti,[69] D. Chakraborty,[49] K. M. Chan,[53] A. Chandra,[77] E. Chapon,[17] G. Chen,[55] S. Chevalier-Théry,[17] D. K. Cho,[74] S. W. Cho,[30] S. Choi,[30] B. Choudhary,[27] S. Cihangir,[47] D. Claes,[63] J. Clutter,[55] M. Cooke,[47] W. E. Cooper,[47] M. Corcoran,[77] F. Couderc,[17] M.-C. Cousinou,[14] A. Croc,[17] D. Cutts,[74] A. Das,[44] G. Davies,[42] K. De,[75] S. J. de Jong,[33] E. De La Cruz-Burelo,[31] F. Déliot,[17] M. Demarteau,[47] R. Demina,[68] D. Denisov,[47] S. P. Denisov,[37] S. Desai,[47] C. Deterre,[17] K. DeVaughan,[63] H. T. Diehl,[47] M. Diesburg,[47] P. F. Ding,[43] A. Dominguez,[63] T. Dorland,[79] A. Dubey,[27] L. V. Dudko,[36] D. Duggan,[64] A. Duperrin,[14] S. Dutt,[26] A. Dyshkant,[49] M. Eads,[63] D. Edmunds,[61] P. Eller,[48,††] J. Ellison,[45] V. D. Elvira,[47] Y. Enari,[16] H. Evans,[51] A. Evdokimov,[70] V. N. Evdokimov,[37] G. Facini,[59] T. Ferbel,[68] F. Fiedler,[23] F. Filthaut,[33] W. Fisher,[61] H. E. Fisk,[47] C. Focke,[48,††] M. Fortner,[49] H. Fox,[41] S. Fuess,[47] A. Garcia-Bellido,[68] G. A. García-Guerra,[31,‡] V. Gavrilov,[35] P. Gay,[12] W. Geng,[14,61] D. Gerbaudo,[65] C. E. Gerber,[48] Y. Gershtein,[64] G. Ginther,[47,68] G. Golovanov,[34] A. Goussiou,[79] P. D. Grannis,[69] S. Greder,[18] H. Greenlee,[47] Z. D. Greenwood,[57] E. M. Gregores,[4] G. Grenier,[19] Ph. Gris,[12] J.-F. Grivaz,[15] A. Grohsjean,[17] S. Grünendahl,[47] M. W. Grünewald,[29] T. Guillemin,[15] G. Gutierrez,[47] P. Gutierrez,[72] A. Haas,[67,§] S. Hagopian,[46] J. Haley,[59] L. Han,[6] K. Harder,[43] A. Harel,[68] J. M. Hauptman,[54] J. Hays,[42] T. Head,[43] T. Hebbeker,[20] D. Hedin,[49] H. Hegab,[73] A. P. Heinson,[45] U. Heintz,[74] C. Hensel,[22] I. Heredia-De La Cruz,[31] K. Herner,[60] G. Hesketh,[43,‖] M. D. Hildreth,[53] R. Hirosky,[78] T. Hoang,[46] J. D. Hobbs,[69] B. Hoeneisen,[11] M. Hohlfeld,[23] Z. Hubacek,[9,17] N. Huske,[16] V. Hynek,[9] I. Iashvili,[66] Y. Ilchenko,[76] R. Illingworth,[47] A. S. Ito,[47] S. Jabeen,[74] M. Jaffré,[15] D. Jamin,[14] A. Jayasinghe,[72] R. Jesik,[42] K. Johns,[44] M. Johnson,[47] A. Jonckheere,[47] P. Jonsson,[42] J. Joshi,[26] A. W. Jung,[47] A. Juste,[39] K. Kaadze,[56] E. Kajfasz,[14] D. Karmanov,[36] P. A. Kasper,[47] I. Katsanos,[63] R. Kehoe,[76] S. Kermiche,[14] N. Khalatyan,[47] A. Khanov,[73] A. Kharchilava,[66] Y. N. Kharzheev,[34] J. M. Kohli,[26] A. V. Kozelov,[37] J. Kraus,[61] S. Kulikov,[37] A. Kumar,[66] A. Kupco,[10] T. Kurča,[19] V. A. Kuzmin,[36] J. Kvita,[8] S. Lammers,[51] G. Landsberg,[74] P. Lebrun,[19] H. S. Lee,[30] S. W. Lee,[54] W. M. Lee,[47] J. Lellouch,[16] L. Li,[45] Q. Z. Li,[47] S. M. Lietti,[5] J. K. Lim,[30] D. Lincoln,[47] J. Linnemann,[61] V. V. Lipaev,[37] R. Lipton,[47] Y. Liu,[6] A. Lobodenko,[38] M. Lokajicek,[10] R. Lopes de Sa,[69] H. J. Lubatti,[79] R. Luna-Garcia,[31,¶] A. L. Lyon,[47] A. K. A. Maciel,[2] D. Mackin,[77] R. Madar,[17] R. Magaña-Villalba,[31] S. Malik,[63] V. L. Malyshev,[34] Y. Maravin,[56] J. Martínez-Ortega,[31] R. McCarthy,[69] C. L. McGivern,[55] M. M. Meijer,[33] A. Melnitchouk,[62] D. Menezes,[49] P. G. Mercadante,[4] M. Merkin,[36] A. Meyer,[20] J. Meyer,[22] F. Miconi,[18] N. K. Mondal,[28] G. S. Muanza,[14] M. Mulhearn,[78] E. Nagy,[14] M. Naimuddin,[27] M. Narain,[74] R. Nayyar,[27] H. A. Neal,[60] J. P. Negret,[7] P. Neustroev,[38] S. F. Novaes,[5] T. Nunnemann,[24] G. Obrant,[38,‡‡] J. Orduna,[77] N. Osman,[14] J. Osta,[53] G. J. Otero y Garzón,[1] M. Padilla,[45] A. Pal,[75] N. Parashar,[52] V. Parihar,[74] S. K. Park,[30] J. Parsons,[67] R. Partridge,[74,§] N. Parua,[51] A. Patwa,[70] B. Penning,[47] M. Perfilov,[36] K. Peters,[43] Y. Peters,[43] K. Petridis,[43] G. Petrillo,[68] P. Pétroff,[15] R. Piegaia,[1] M.-A. Pleier,[70] P. L. M. Podesta-Lerma,[31,**] V. M. Podstavkov,[47] P. Polozov,[35] A. V. Popov,[37] M. Prewitt,[77] D. Price,[51] N. Prokopenko,[37] H. B. Prosper,[46] S. Protopopescu,[70] J. Qian,[60] A. Quadt,[22] B. Quinn,[62] M. S. Rangel,[2] K. Ranjan,[27] P. N. Ratoff,[41] I. Razumov,[37] P. Renkel,[76] M. Rijssenbeek,[69] I. Ripp-Baudot,[18] F. Rizatdinova,[73] M. Rominsky,[47] A. Ross,[41] C. Royon,[17] P. Rubinov,[47] R. Ruchti,[53] G. Safronov,[35] G. Sajot,[13] P. Salcido,[49] A. Sánchez-Hernández,[31] M. P. Sanders,[24] B. Sanghi,[47] A. S. Santos,[5] G. Savage,[47] L. Sawyer,[57] T. Scanlon,[42] R. D. Schamberger,[69] Y. Scheglov,[38] H. Schellman,[50] T. Schliephake,[25] S. Schlobohm,[79] C. Schwanenberger,[43] R. Schwienhorst,[61] J. Sekaric,[55] H. Severini,[72] E. Shabalina,[22] V. Shary,[17] A. A. Shchukin,[37] R. K. Shivpuri,[27] V. Simak,[9] V. Sirotenko,[47] P. Skubic,[72] P. Slattery,[68] D. Smirnov,[53] K. J. Smith,[66] G. R. Snow,[63] J. Snow,[71] S. Snyder,[70] S. Söldner-Rembold,[43] L. Sonnenschein,[20] K. Soustruznik,[8] J. Stark,[13] V. Stolin,[35] D. A. Stoyanova,[37] M. Strauss,[72] D. Strom,[48] L. Stutte,[47] L. Suter,[43] P. Svoisky,[72] M. Takahashi,[43] A. Tanasijczuk,[1] M. Titov,[17] V. V. Tokmenin,[34] N. Triplett,[54] Y.-T. Tsai,[68] K. Tschann-Grimm,[69] D. Tsybychev,[69] B. Tuchming,[17] C. Tully,[65] L. Uvarov,[38] S. Uvarov,[38] S. Uzunyan,[49] R. Van Kooten,[51] W. M. van Leeuwen,[32] N. Varelas,[48] E. W. Varnes,[44]

I. A. Vasilyev,[37] P. Verdier,[19] L. S. Vertogradov,[34] M. Verzocchi,[47] M. Vesterinen,[43] D. Vilanova,[17] P. Vokac,[9] H. D. Wahl,[46] M. H. L. S. Wang,[47] J. Warchol,[53] G. Watts,[79] M. Wayne,[53] M. Weber,[47,††] L. Welty-Rieger,[50] A. White,[75] D. Wicke,[25] M. R. J. Williams,[41] G. W. Wilson,[55] M. Wobisch,[57] D. R. Wood,[59] T. R. Wyatt,[43] Y. Xie,[47] C. Xu,[60] S. Yacoob,[50] R. Yamada,[47] W.-C. Yang,[43] T. Yasuda,[47] Y. A. Yatsunenko,[34] Z. Ye,[47] H. Yin,[47] K. Yip,[70] S. W. Youn,[47] J. Yu,[75] S. Zelitch,[78] T. Zhao,[79] B. Zhou,[60] J. Zhu,[60] M. Zielinski,[68] D. Zieminska,[51] and L. Zivkovic[74]

(The D0 Collaboration)

[1]*Universidad de Buenos Aires, Buenos Aires, Argentina*
[2]*LAFEX, Centro Brasileiro de Pesquisas Físicas, Rio de Janeiro, Brazil*
[3]*Universidade do Estado do Rio de Janeiro, Rio de Janeiro, Brazil*
[4]*Universidade Federal do ABC, Santo André, Brazil*
[5]*Instituto de Física Teórica, Universidade Estadual Paulista, São Paulo, Brazil*
[6]*University of Science and Technology of China, Hefei, People's Republic of China*
[7]*Universidad de los Andes, Bogotá, Colombia*
[8]*Charles University, Faculty of Mathematics and Physics, Center for Particle Physics, Prague, Czech Republic*
[9]*Czech Technical University in Prague, Prague, Czech Republic*
[10]*Center for Particle Physics, Institute of Physics, Academy of Sciences of the Czech Republic, Prague, Czech Republic*
[11]*Universidad San Francisco de Quito, Quito, Ecuador*
[12]*LPC, Université Blaise Pascal, CNRS/IN2P3, Clermont, France*
[13]*LPSC, Université Joseph Fourier Grenoble 1, CNRS/IN2P3, Institut National Polytechnique de Grenoble, Grenoble, France*
[14]*CPPM, Aix-Marseille Université, CNRS/IN2P3, Marseille, France*
[15]*LAL, Université Paris-Sud, CNRS/IN2P3, Orsay, France*
[16]*LPNHE, Universités Paris VI and VII, CNRS/IN2P3, Paris, France*
[17]*CEA, Irfu, SPP, Saclay, France*
[18]*IPHC, Université de Strasbourg, CNRS/IN2P3, Strasbourg, France*
[19]*IPNL, Université Lyon 1, CNRS/IN2P3, Villeurbanne, France and Université de Lyon, Lyon, France*
[20]*III. Physikalisches Institut A, RWTH Aachen University, Aachen, Germany*
[21]*Physikalisches Institut, Universität Freiburg, Freiburg, Germany*
[22]*II. Physikalisches Institut, Georg-August-Universität Göttingen, Göttingen, Germany*
[23]*Institut für Physik, Universität Mainz, Mainz, Germany*
[24]*Ludwig-Maximilians-Universität München, München, Germany*
[25]*Fachbereich Physik, Bergische Universität Wuppertal, Wuppertal, Germany*
[26]*Panjab University, Chandigarh, India*
[27]*Delhi University, Delhi, India*
[28]*Tata Institute of Fundamental Research, Mumbai, India*
[29]*University College Dublin, Dublin, Ireland*
[30]*Korea Detector Laboratory, Korea University, Seoul, Korea*
[31]*CINVESTAV, Mexico City, Mexico*
[32]*Nikhef, Science Park, Amsterdam, the Netherlands*
[33]*Radboud University Nijmegen, Nijmegen, the Netherlands and Nikhef, Science Park, Amsterdam, the Netherlands*
[34]*Joint Institute for Nuclear Research, Dubna, Russia*
[35]*Institute for Theoretical and Experimental Physics, Moscow, Russia*
[36]*Moscow State University, Moscow, Russia*
[37]*Institute for High Energy Physics, Protvino, Russia*
[38]*Petersburg Nuclear Physics Institute, St. Petersburg, Russia*
[39]*Institució Catalana de Recerca i Estudis Avançats (ICREA) and Institut de Física d'Altes Energies (IFAE), Barcelona, Spain*
[40]*Stockholm University, Stockholm and Uppsala University, Uppsala, Sweden*
[41]*Lancaster University, Lancaster LA1 4YB, United Kingdom*
[42]*Imperial College London, London SW7 2AZ, United Kingdom*
[43]*The University of Manchester, Manchester M13 9PL, United Kingdom*
[44]*University of Arizona, Tucson, Arizona 85721, USA*
[45]*University of California Riverside, Riverside, California 92521, USA*
[46]*Florida State University, Tallahassee, Florida 32306, USA*
[47]*Fermi National Accelerator Laboratory, Batavia, Illinois 60510, USA*
[48]*University of Illinois at Chicago, Chicago, Illinois 60607, USA*
[49]*Northern Illinois University, DeKalb, Illinois 60115, USA*
[50]*Northwestern University, Evanston, Illinois 60208, USA*
[51]*Indiana University, Bloomington, Indiana 47405, USA*

[52]Purdue University Calumet, Hammond, Indiana 46323, USA
[53]University of Notre Dame, Notre Dame, Indiana 46556, USA
[54]Iowa State University, Ames, Iowa 50011, USA
[55]University of Kansas, Lawrence, Kansas 66045, USA
[56]Kansas State University, Manhattan, Kansas 66506, USA
[57]Louisiana Tech University, Ruston, Louisiana 71272, USA
[58]Boston University, Boston, Massachusetts 02215, USA
[59]Northeastern University, Boston, Massachusetts 02115, USA
[60]University of Michigan, Ann Arbor, Michigan 48109, USA
[61]Michigan State University, East Lansing, Michigan 48824, USA
[62]University of Mississippi, University, Mississippi 38677, USA
[63]University of Nebraska, Lincoln, Nebraska 68588, USA
[64]Rutgers University, Piscataway, New Jersey 08855, USA
[65]Princeton University, Princeton, New Jersey 08544, USA
[66]State University of New York, Buffalo, New York 14260, USA
[67]Columbia University, New York, New York 10027, USA
[68]University of Rochester, Rochester, New York 14627, USA
[69]State University of New York, Stony Brook, New York 11794, USA
[70]Brookhaven National Laboratory, Upton, New York 11973, USA
[71]Langston University, Langston, Oklahoma 73050, USA
[72]University of Oklahoma, Norman, Oklahoma 73019, USA
[73]Oklahoma State University, Stillwater, Oklahoma 74078, USA
[74]Brown University, Providence, Rhode Island 02912, USA
[75]University of Texas, Arlington, Texas 76019, USA
[76]Southern Methodist University, Dallas, Texas 75275, USA
[77]Rice University, Houston, Texas 77005, USA
[78]University of Virginia, Charlottesville, Virginia 22901, USA
[79]University of Washington, Seattle, Washington 98195, USA

(Received 17 August 2011; published 5 December 2011)

We present measurements of production cross sections of single top quarks in $p\bar{p}$ collisions at $\sqrt{s} = 1.96$ TeV in a data sample corresponding to an integrated luminosity of 5.4 fb^{-1} collected by the D0 detector at the Fermilab Tevatron Collider. We select events with an isolated electron or muon, an imbalance in transverse energy, and two, three, or four jets, with one or two of them containing a bottom hadron. We obtain an inclusive cross section of $\sigma(p\bar{p} \to tb + X, tqb + X) = 3.43 \pm^{0.73}_{0.74}$ pb and use it to extract the CKM matrix element $0.79 < |V_{tb}| \leq 1$ at the 95% C.L. We also measure $\sigma(p\bar{p} \to tb + X) = 0.68 \pm^{0.38}_{0.35}$ pb and $\sigma(p\bar{p} \to tqb + X) = 2.86 \pm^{0.69}_{0.63}$ pb when assuming, respectively, tqb and tb production rates as predicted by the standard model.

DOI: 10.1103/PhysRevD.84.112001 PACS numbers: 14.65.Ha, 12.15.Hh, 12.15.Ji, 13.85.Qk

I. INTRODUCTION

Top quarks are produced at hadron colliders as $t\bar{t}$ pairs via the strong interaction or singly via the electroweak interaction [1,2]. Because of the larger production rate and higher signal-to-background ratio, the production of $t\bar{t}$ pairs is better studied and indeed it was through the $t\bar{t}$ production process that the existence of the top quark was established in 1995 at the Fermilab Tevatron Collider [3,4]. The observation of the single top quark production, however, was possible after CDF and D0 collaborations accumulated ≈ 50 times more integrated luminosity than what was needed for observation of top quarks in $t\bar{t}$ production [5,6]. Single top quark events are produced at about half of the rate of top quark pairs and with lower jet multiplicities, and therefore their study is more susceptible to contamination from background processes.

Electroweak production of top quarks at the Tevatron proceeds mainly via the decay of a timelike virtual W boson accompanied by a bottom quark in the s channel ($tb = t\bar{b} + \bar{t}b$) [7] or via the exchange of a spacelike virtual W boson between a light quark and a bottom quark in the t channel ($tqb = tq\bar{b} + \bar{t}qb$, where q refers to the

*with visitors from Augustana College, Sioux Falls, SD, USA
†with visitors from The University of Liverpool, Liverpool, UK
‡with visitors from UPIITA-IPN, Mexico City, Mexico
§with visitors from SLAC, Menlo Park, CA, USA
‖with visitors from University College London, London, UK
¶with visitors from Centro de Investigacion en Computacion—IPN, Mexico City, Mexico
**with visitors from ECFM, Universidad Autonoma de Sinaloa, Culiacán, Mexico
††with visitors from Universität Bern, Bern, Switzerland
‡‡Deceased

light quark or antiquark) [8,9]. Figure 1 shows the lowest level Feynman diagrams for *s*- and *t*-channel production [10]. A third process *tW*, in which the top quark is produced together with a *W* boson, has a small cross section at the Tevatron [2] and is therefore not considered in this analysis.

Single top quark events can be used to probe the *Wtb* vertex and to directly measure the magnitude of the Cabibbo-Kobayashi-Maskawa (CKM) [11] quark mixing matrix element $|V_{tb}|$. Under the assumptions that there are only three quark generations and that the CKM matrix is unitary, the matrix elements are severely constrained [12]: $|V_{td}| = (8.62^{+0.26}_{-0.20}) \times 10^{-3}$, $|V_{ts}| = (4.03^{+0.11}_{-0.07}) \times 10^{-4}$, and $|V_{tb}| = 0.999152^{+0.000030}_{-0.000045}$. However, in several extensions of the standard model (SM) involving, for instance, a fourth generation of quarks or an additional heavy quark singlet that mixes with the top quark, $|V_{tb}|$ can be significantly smaller than unity [13]. A direct determination of $|V_{tb}|$, without assuming unitarity or three generations, is possible through the measurement of the total single top quark production cross section [14]. The current measured value for the total single top quark cross section is $2.76^{+0.58}_{-0.47}$ pb at $\sqrt{s} = 1.96$ TeV, resulting in $|V_{tb}| = 0.88 \pm 0.07$ with a limit of $|V_{tb}| > 0.77$ at the 95% C.L. assuming a top quark mass $m_t = 170$ GeV [15].

Previous measurements of single top quark production cross sections at the Tevatron [5,6,16–19] included events from both the *tb* and *tqb* processes, assuming a ratio of cross sections [2] for the two processes based on the SM. Similarly, a recent measurement of the *tqb* production rate at the LHC [20] assumes SM production for the *tb* and *tW* processes. However, different modes of single top quark production are sensitive to different manifestations of physics beyond the SM. Examples include models with additional quark generations [13], new heavy bosons [21–23], flavor-changing neutral currents (FCNC) [21,24], or anomalous top quark couplings [25–27]. It is therefore important to also measure the individual *tb* and *tqb* production rates, which together represent a comprehensive probe of the interactions of the top quark.

Using data corresponding to 5.4 fb^{-1} of integrated luminosity recorded with the D0 detector [28], we present an improved measurement of the production rate of $tb + tqb$. We also present measurements of the production rates of the individual *tb* and *tqb* processes performed assuming, respectively, *tqb* and *tb* production rates as predicted by the SM. Finally, we present a new direct measurement of $|V_{tb}|$ extracted from the measured $tb + tqb$ cross section.

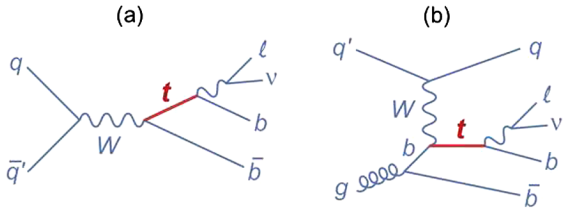

FIG. 1 (color online). [color online] Lowest level Feynman diagrams for (a) *tb* and (b) *tqb* single top quark production.

II. EVENT SELECTION

This analysis extends previous work by the D0 Collaboration [6,16,17,29] and uses the same data, event selection, and modeling of signal and background as in Ref. [30]. It differs however, in the assumptions used to extract the cross sections of the individual *tb* and *tqb* production modes.

The data were collected with a logical OR of many trigger conditions, which together are fully efficient for the single top quark signal that passes the event selection described below. We select events containing only one isolated electron or muon with high transverse momentum (p_T) and having a large imbalance in the transverse energy ($\not\!\!E_T$) indicative of the presence of a neutrino. Events originating from single top quark production are expected to contain at least one *b* quark jet from the decay of the top quark and a second *b* quark jet in the *s* channel, or a light quark jet and a spectator *b* quark jet for the *t* channel. In both cases, gluon radiation can give rise to additional jets. Events are selected with two, three, or four jets reconstructed using a cone algorithm [31] in (y, ϕ) space, where *y* is the rapidity and ϕ is the azimuthal angle, and the cone radius 0.5. The jets must satisfy the following conditions: leading jet $p_T > 25$ GeV, other jets with $p_T > 15$ GeV, and with pseudorapidities of all jets $|\eta| < 3.4$. Requirements are also placed on $\not\!\!E_T$: $20 < \not\!\!E_T < 200$ GeV for events with two jets, and $25 < \not\!\!E_T < 200$ GeV for events with three or four jets. The maximum $\not\!\!E_T$ requirement removes events that suffer from poor modeling of the high energy tail of the muon momentum resolution. We require one isolated electron with $|\eta| < 1.1$ and $p_T > 15(20)$ GeV for events with two (three or four) jets, or one isolated muon with $|\eta| < 2.0$ and $p_T > 15$ GeV.

The sample resulting from this selection is dominated by *W* bosons produced in association with jets (W + jets), with smaller contributions from $t\bar{t}$ pairs decaying into the single lepton plus jets final state or the dilepton final state when one lepton or some jets are not reconstructed. Multijet events also contribute to the background when a jet is misidentified as an isolated electron or a heavy-flavor quark decays to a muon that satisfies isolation criteria, in combination with misreconstruction of $\not\!\!E_T$. Diboson (*WW*, *WZ*, *ZZ*) and Z + jets processes contribute only marginally to the total background but are taken into account. The background from multijets is kept small ($< 6\%$) by requiring that the total scalar sum (H_T) of the transverse momenta of the final-state objects (lepton, $\not\!\!E_T$, and jets) be larger than 120/140/160 GeV for events with 2/3/4 jets, and that the $\not\!\!E_T$ does not point along the transverse direction of the lepton or the leading jet. Soft-scattering

processes are suppressed by requiring a minimum value for the total scalar sum of the p_T of the jets [H_T(alljets)] ranging from 50 to 100 GeV, depending on the number of jets in an event and the data collection period.

To enhance the signal fraction, one or two of the jets are required to contain long-lived bottom hadrons (b jets), as determined through a multivariate b-tagging algorithm [32]. This algorithm uses several variables to discriminate b jets from other jets such as: (i) decay length significance of the secondary vertex, (ii) the χ^2 per degree of freedom of the secondary vertex fit, (iii) weighted combination of the tracks' impact parameter significances, (iv) probability that the jet originates from the primary $p\bar{p}$ interaction vertex, (v) number of tracks used to reconstruct the secondary vertex, (vi) mass of the secondary vertex, and (vii) number of secondary vertices found inside the jet. To improve sensitivity to signal, the samples are divided into six independent analysis channels, depending on the jet multiplicity (two, three, or four jets), and the number of b-tagged jets (one or two). The efficiency of the event selection, including branching fraction and the b-tagging requirements, is $(2.9 \pm 0.4)\%$ for tb and $(2.0 \pm 0.3)\%$ for tqb. The tqb process has a lower acceptance than the tb channel because the second b-jet has low transverse momentum and is difficult to identify. We apply additional requirements to select two control samples used to test whether the background model reproduces the data in regions dominated by one specific type of background. The control sample dominated by W + jets is required to have exactly two jets, $H_T < 175$ GeV, and only one b-tagged jet where W + jets events constitute 82% of this sample, and the $t\bar{t}$ component is less than 2%. The control sample dominated by $t\bar{t}$ is required to have exactly four jets, $H_T > 300$ GeV, and one or two b-tagged jets where $t\bar{t}$ events constitute 84% of the sample, and the W + jets component is 12%.

III. MODELS FOR SIGNAL AND BACKGROUND

Single top quark events are modeled for a top quark mass $m_t = 172.5$ GeV using the COMPHEP-based effective next-to-leading order (NLO) Monte Carlo (MC) event generator SINGLETOP [33], which preserves spin information in the decays of the top quark and the W boson and provides event kinematics that reproduce distributions predicted by NLO calculations [34,35]. The $t\bar{t}$, W + jets, and Z + jets events are simulated with the ALPGEN leading order MC generator [36]. Diboson processes are modeled using PYTHIA [37]. For all these MC samples, PYTHIA is also used to evolve parton showers and to model proton remnants and hadronization of all generated partons. The presence of additional $p\bar{p}$ interactions is modeled by events selected from random beam crossings matching the instantaneous luminosity profile in the data. All MC events are passed through a GEANT-based simulation [38] of the D0 detector.

Differences between simulation and data in lepton and jet reconstruction efficiencies and resolutions, jet energy scale, and b-tagging efficiencies are corrected in the simulation by applying correction functions measured from separate data samples. Comparisons of ALPGEN with data and with other generators show small discrepancies in distributions of jet pseudorapidity and angular separations between jets [39]. We therefore correct the ALPGEN W + jets and Z + jets samples by sequentially applying polynomial reweighting functions parameterized by the leading and second-leading jet η, $\Delta R = \sqrt{(\Delta\phi)^2 + (\Delta\eta)^2}$ between the two leading jets, and third- and fourth-leading jet η, if applicable. These functions are derived from the ratio between the number of W + jets and Z + jets events observed in data and the event yields predicted by MC. After these corrections, the MC description is in good agreement with our high statistics sample of events prior to the application of b-tagging. The multijet background is modeled using the selection discussed in Sec. II, but choosing events that fail isolation criteria for leptons.

MC samples are scaled to the theoretical cross section at approximately NNLO [1] for $t\bar{t}$, and NLO [40] for Z + jets and diboson cases. The contributions from W + jets and multijet are normalized by comparing the prediction for background to data before b-tagging. We use a procedure that relies on three distributions [lepton p_T, $\not\!\!E_T$, and W reconstructed mass in the transverse plane $M_T(W)$] that have distinctive shapes for W + jets and multijets events and are thus sensitive to their relative contributions in the selected sample. The normalization scale factors for W + jets ($\lambda_{W\,\mathrm{jets}}$) and multijet ($\lambda_{\mathrm{multijets}}$) are constrained by the following equation:

$$N = \lambda_{W\,\mathrm{jets}} N_{W\,\mathrm{jets}} + \lambda_{\mathrm{multijets}} N_{\mathrm{multijets}}, \quad (1)$$

where $N = N_{\mathrm{data}} - N_{\mathrm{non}\text{-}W\,\mathrm{jets}}$ and N_{data}, $N_{\mathrm{non}\text{-}W\,\mathrm{jets}}$, $N_{W\,\mathrm{jets}}$, and $N_{\mathrm{multijets}}$ are the event yields in data, non-W + jets MC, W + jets, and multijet samples, respectively. The W + jets sample contains events with light flavor (Wjj, $j = u, d, s$) and heavy flavor (Wjc, $Wc\bar{c}$, and $Wb\bar{b}$) quarks. The non-W + jets MC samples include single top quark, $t\bar{t}$, Z + jets, and diboson production. The values of $\lambda_{W\,\mathrm{jets}}$ and $\lambda_{\mathrm{multijets}}$ are varied to maximize the product of the Kolmogorov-Smirnov test values [41] for the three kinematic distributions. This procedure is done separately for events with two, three, and four jets and for each lepton flavor. After the normalization, the total sum of the W + jets and multijets yields plus the small contributions from $t\bar{t}$, single top, Z + jets, and diboson production equals the total data yield for each of the six analysis channels.

Without modifying the overall normalization of the W + jets MC sample, we apply an additional scale factor to W and Z boson events produced in conjunction with heavy-flavor jets (b or c) to match NLO calculations [40]: $Wb\bar{b}$ and $Wc\bar{c}$ by 1.47, $Zb\bar{b}$ by 1.52, $Zc\bar{c}$ by 1.67, and

Wcj by 1.32. We evaluate whether an additional normalization factor $\lambda_{\rm HF}$ is required for the $Wb\bar{b}$ and $Wc\bar{c}$ samples by using events with two jets that pass the event selection described in Sec. II but fail the b-tagging requirements (zero-tag sample). The zero-tag sample has no overlap with the sample used to measure the single top quark cross section. During this study, we keep the normalization of the $W+$jets sample fixed to the value obtained by the iterative method described above and derive $\lambda_{\rm HF}$ with the following equation:

$$N^{(0)} = N^{(0)}_{Wlp} + \lambda_{\rm HF} N^{(0)}_{Whp}, \quad (2)$$

where $N = N_{\rm data} - N_{\rm multijets} - N_{\text{non-Wjets}}$, $N_{Wlp} = N_{Wjj} + N_{Wcj}$, and $N_{Whp} = N_{Wcc} + N_{Wbb}$. The superscript (0) indicates that the equation is written for the zero-tag sample defined above. The measured value of $\lambda_{\rm HF}$ is consistent with one. Uncertainties on the assumed cross sections for single top quark, $t\bar{t}$, and Wcj production and the cross section ratio of $Wc\bar{c}$ to $Wb\bar{b}$ are taken into account. As expected, $\lambda_{\rm HF}$ is most affected by variations on the Wcj cross section and the $Wc\bar{c}$ to $Wb\bar{b}$ cross section ratio. An estimated uncertainty of 12% is assigned to the normalization of the $Wc\bar{c}$ and $Wb\bar{b}$ MC samples based on this study.

We also consider other sources of systematic uncertainty from modeling both the background and signal. These uncertainties usually affect the normalization and, in some cases, also the shape of the distributions. The largest uncertainties arise from the jet energy scale (0.3–14.6)%, jet energy resolution (0.2–11.6)%, and corrections to b-tagging efficiencies (6.6–21.2)%. There are also contributions due to limited statistics of the MC samples 6.0%, the measured luminosity 6.1%, and uncertainties on the trigger modeling 5.0%.

Table I lists the numbers of expected and observed events for each process after event selection, including b-tagging. The procedure for normalizing the $W+$jets and multijet backgrounds constrains the total predicted background to match the data before b-tagging, but variations in tagging rates allow differences in event counts after tagging. Figure 2 shows comparisons between data and simulation before and after applying b-tagging. In the same figure, the normalization and differential spectra of the two dominant backgrounds are checked using the control samples dominated by $W+$jets (e), and by $t\bar{t}$ (f) events. These plots are indicative of the adequate background modeling attained for various sample conditions in the analysis.

TABLE I. Numbers of expected and observed events in a data sample corresponding to 5.4 fb^{-1} of integrated luminosity, with uncertainties including both statistical and systematic components. The tb and tqb contributions are normalized to their SM expectations for a top quark mass of 172.5 GeV.

Source	2 jets	3 jets	4 jets
tb	104 ± 16	44 ± 7.8	13 ± 3.5
tqb	140 ± 13	72 ± 9.4	26 ± 6.4
$t\bar{t}$	433 ± 87	830 ± 133	860 ± 163
$W+$jets	$3,560 \pm 354$	$1,099 \pm 169$	284 ± 76
$Z+$jets & dibosons	400 ± 55	142 ± 41	35 ± 18
Multijets	277 ± 34	130 ± 17	43 ± 5.2
Sum of above sources	$4,914 \pm 558$	$2,317 \pm 377$	$1,261 \pm 272$
Data	4881	2307	1283

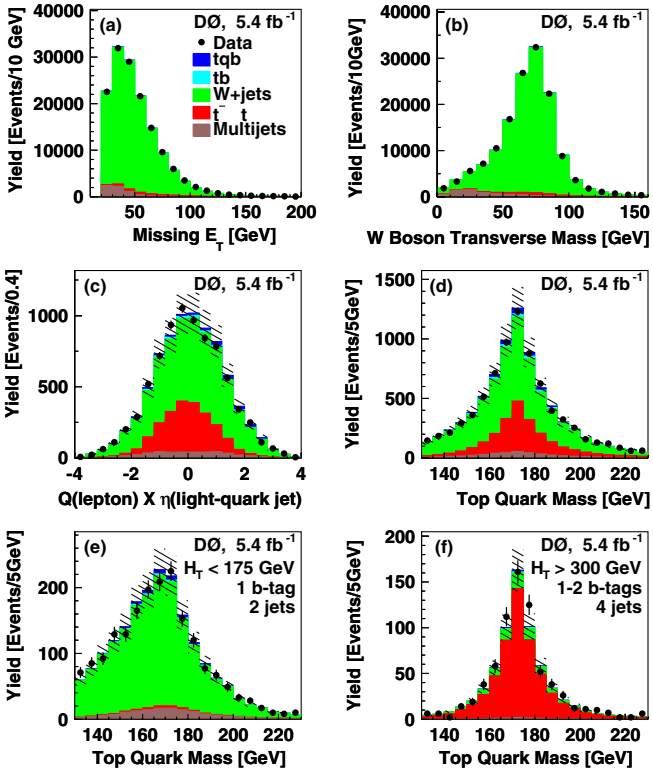

FIG. 2 (color online). [color online] Comparisons between the data and the background model for (a) $\not\!\!E_T$, (b) W boson transverse mass before b-tagging, and (c) light quark jet pseudorapidity multiplied by lepton charge, after b-tagging. Reconstructed top quark mass (d) after b-tagging, (e) in a control sample dominated by $W+$jets, and (f) in a control sample dominated by $t\bar{t}$. The hatched bands show the $\pm 1\sigma$ uncertainty (normalization and shape) on the background prediction for distributions obtained after b-jet identification (c–f). The $W+$jets contribution includes events from $Z+$jets and diboson sources.

IV. MULTIVARIATE ANALYSES

Since the expected single top quark contribution is smaller than the uncertainty on the background, we use multivariate analysis (MVA) methods to extract the signal. The application of these methods to the measurement of the single top quark production cross section is described in Ref. [17]. Three different MVA techniques are used in this analysis: (i) Bayesian neural networks (BNN) [42],

(ii) boosted decision trees (BDT) [43], and (iii) neuroevolution of augmented topologies (NEAT) [44]. Each MVA method constructs a function that approximates the probability $\Pr(S|\mathbf{x})$ that an event, characterized by the variables $\mathbf{x}$, originates from the signal process, $S = \{tb, tqb, tb + tqb\}$. Therefore, each method defines a discriminant D that can be used to constrain the uncertainties of the background in the low-discriminant region $D \approx 0$ and extract a signal from an excess in the high-discriminant region $D \approx 1$. All three methods use the same data and model for background, performing the analyses separately on the six mutually exclusive subsamples defined before. All three methods also consider the same sources of systematic uncertainty, and are trained using variables for discriminating signal from background chosen from a common set of well-modeled variables [17,45]. These variables can be classified in five categories: single object kinematics, global event kinematics, jet reconstruction, top quark reconstruction, and angular correlations. The BNN uses four-vectors of the lepton and jets and a two-vector for $\not\!\!E_T$ to build the discriminant. The BNN performance is improved by adding variables containing the lepton charge and b-tagging information, resulting in 14, 18, and 22 variables for events with 2, 3, and 4 jets. The BDT ranks and selects the best 50 variables for all the analysis channels, while NEAT uses the TMVA [46] implementation of the "RuleFit" [47] algorithm to select the best 30 variables in each channel.

Each MVA method is trained separately for the two single top quark production channels: (i) for the tb discriminants, with tb considered signal and tqb treated as a part of the background, and (ii) for tqb discriminants, with tqb considered signal and tb treated as a part of the background.

Using ensembles of data sets containing contributions from background and SM signal, we infer that the correlation among the outputs of the individual MVA methods is $\approx 70\%$. An increase in sensitivity can therefore be obtained by combining these methods to form a new discriminant [6]. To achieve the maximum sensitivity, a second BNN is used to construct a combined discriminant for each channel, for tb, tqb, and $tb + tqb$ events, defined as B_{tb}, B_{tqb}, and B_{tb+tqb}. The B_{tb} and B_{tqb} discriminants take as inputs the three discriminant outputs of BDT, BNN, and NEAT, and they are trained by assuming tb or tqb as signals, respectively. The combined $tb + tqb$ discriminant (B_{tb+tqb}) takes as input the six discriminant outputs of BDT, BNN, and NEAT that are trained separately for the tb and the tqb signal. The training for B_{tb+tqb} treats the combined $tb + tqb$ contribution as signal with relative production rates predicted by SM. Figure 3 shows the outputs of the B_{tb}, B_{tqb}, and B_{tb+tqb} discriminants, where good agreement is observed over the entire range. In these plots, the bins are sorted and merged ("ranked") as a function of the expected signal-to-background ratio (S:B) such that S:B increases monotonically within the range of the discriminant. For the tqb and $tq + tqb$ discriminants, presence of signal is significant in the plots. For the tb discriminant, the signal presence is not as significant.

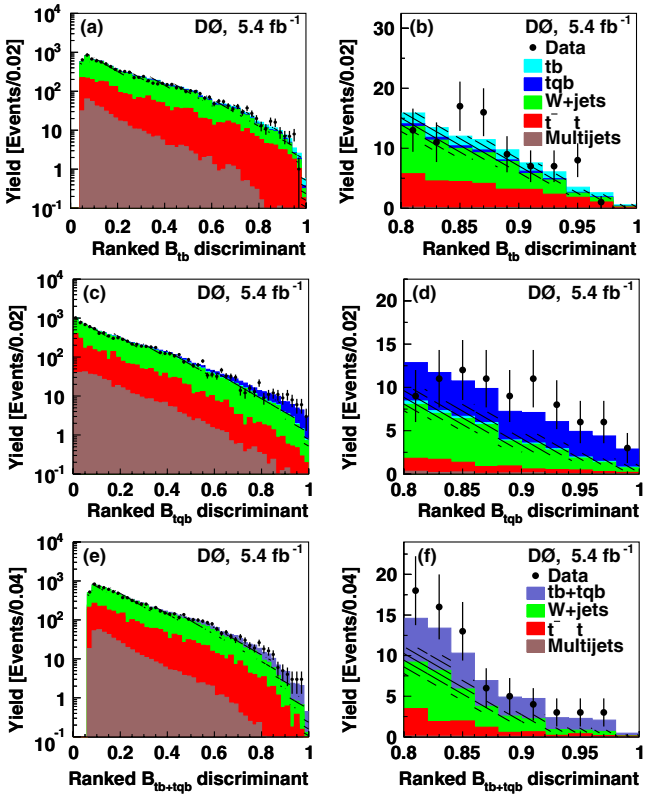

FIG. 3 (color online). [color online] Distributions of the (a) B_{tb}, (c) B_{tqb}, and (e) B_{tb+tqb} discriminants for the entire range [0–1] of the output. Distributions of the (b) B_{tb}, (d) B_{tqb}, and (f) B_{tb+tqb} discriminants for the signal region [0.8–1]. The bins have been ranked by their expected signal-to-background ratio. The tb, tqb, and $tb + tqb$ contributions are normalized to the measured cross sections in Table II. The hatched bands show the $\pm 1\sigma$ uncertainty on the background prediction.

V. MEASURING SIGNAL CROSS SECTIONS

A. Bayesian approach

We use a Bayesian approach [6,16,17] to extract the production cross sections. The method consists of forming a binned likelihood as a product of all six analysis channels (2, 3, or 4 jets with 1 or 2 b-tags) and bins using the full discriminant outputs. We assume a Poisson distribution for the number of events in each bin and uniform prior probabilities for non-negative values of the signal cross sections (tb, tqb, and $tb + tqb$ correspondingly). Systematic uncertainties and their correlations are taken into account by integrating over signal acceptances, background yields, and integrated luminosity, assuming a Gaussian prior for each source of systematic uncertainty. A posterior

probability density as a function of the single top quark cross section is constructed, with the position of the maximum defining the value of the cross section and the width of the distribution in the region that encompasses 68% of the entire area corresponding to the uncertainty (statistical and systematic components combined). The expected cross sections are obtained by setting the number of data events in each channel equal to the value given by the prediction of signal plus background.

B. Ensemble testing

The methods used for extracting the cross sections are validated by studies performed using ensembles of pseudoexperiments that are generated taking into account all systematic uncertainties and their correlations. These ensembles of events are processed through each MVA method for each single top quark production mode and through the same analysis chain as used for the data. Five arbitrary signal cross sections (including the SM prediction) are used to calibrate the tb, tqb, and $tb + tqb$ cross section extraction procedure. Means and standard deviations are determined by fitting Gaussian function to the distributions of extracted values of the measured cross sections in each ensemble. Figure 4 shows the resulting distributions and Gaussian fits for SM ensembles for tb, tqb, and $tb + tqb$ processes. Straight-line fits of the extracted mean cross sections to the input values are shown in Fig. 5, where the shaded bands reflect the standard deviations of the extracted cross sections in each ensemble.

The results of these pseudoexperiments show that the biases on the cross sections are negligible compared to the standard deviations of the extracted values. We therefore do not apply corrections to the measured values of the cross sections in data.

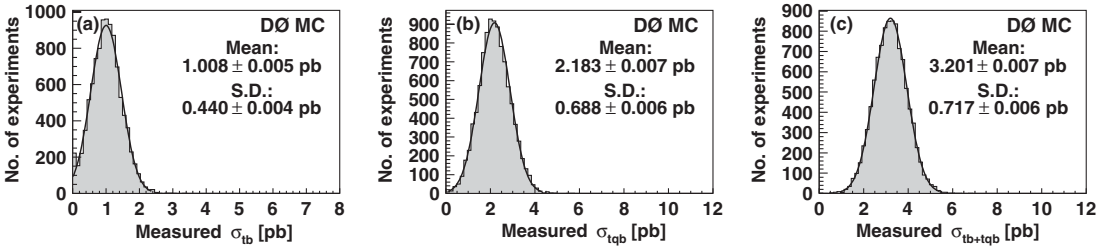

FIG. 4. Distribution and Gaussian fit of the measured cross section in an ensemble of pseudoexperiments with the same integrated luminosity as in data generated assuming the SM for (a) tb, (b) tqb, and (c) $tb + tqb$ processes.

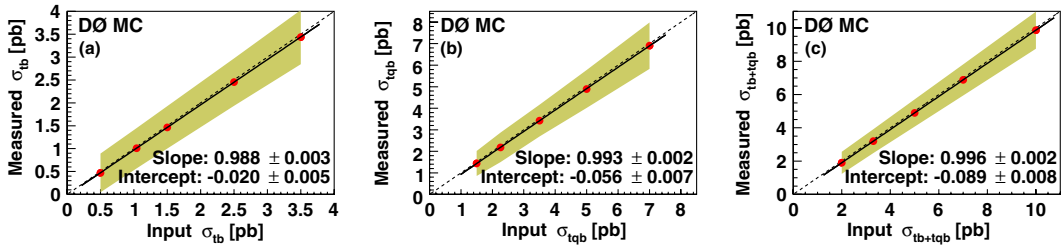

FIG. 5 (color online). [color online] Mean (points) and standard deviation (shaded bands) of cross section as a function of the input cross section for the (a) tb, (b) tqb, and (c) $tb + tqb$ single top quark processes from the ensemble studies of pseudoexperiments with the same integrated luminosity as in data. The continuous lines show the fits to the mean values where their uncertainties are smaller than the size of the points. The dotted lines represent the responses in the case of slope equal one and zero intercept.

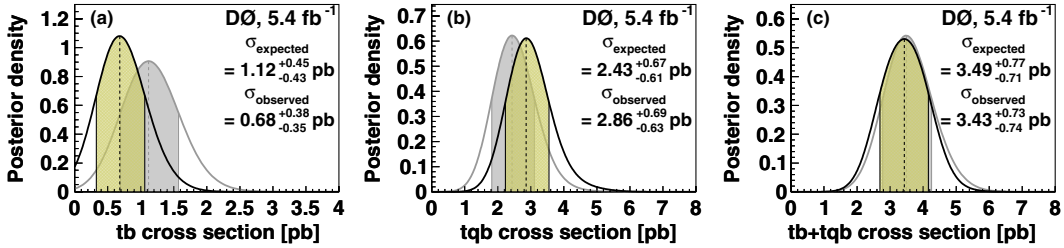

FIG. 6 (color online). [color online] The expected (back) and observed (front) posterior probability densities for (a) tb, (b) tqb, and (c) $tb + tqb$ production. The shaded bands indicate the 68% C.L.s from the peak values.

TABLE II. Expected and observed cross sections in pb for tb, tqb, and $tb + tqb$ production. All results assume a top quark mass of 172.5 GeV.

Discriminant	Expected	Observed
	tb production	
BNN	$1.08^{+0.52}_{-0.50}$	$0.72^{+0.44}_{-0.43}$
BDT	$1.07^{+0.47}_{-0.43}$	$0.68^{+0.41}_{-0.39}$
NEAT	$1.06^{+0.54}_{-0.50}$	$0.17^{+0.41}_{-0.17}$
B_{tb}	$1.12^{+0.45}_{-0.43}$	$0.68^{+0.38}_{-0.35}$
	tqb production	
BNN	$2.49^{+0.76}_{-0.67}$	$2.92^{+0.87}_{-0.73}$
BDT	$2.40^{+0.71}_{-0.66}$	$3.03^{+0.78}_{-0.66}$
NEAT	$2.36^{+0.80}_{-0.77}$	$2.75^{+0.87}_{-0.75}$
B_{tqb}	$2.43^{+0.67}_{-0.61}$	$2.86^{+0.69}_{-0.63}$
	$tb + tqb$ production	
BNN	$3.46^{+0.84}_{-0.78}$	$3.11^{+0.77}_{-0.71}$
BDT	$3.41^{+0.82}_{-0.74}$	$3.01^{+0.80}_{-0.75}$
NEAT	$3.33^{+0.94}_{-0.80}$	$3.59^{+0.96}_{-0.80}$
B_{tb+tqb}	$3.49^{+0.77}_{-0.71}$	$3.43^{+0.73}_{-0.74}$

TABLE III. Dependence on m_t of the measured cross sections in pb for tb, tqb, and $tb + tqb$ production, using the combined discriminants for the assumed top quark masses. The predicted cross sections [2] in pb are also included in the table and labeled "SM."

m_t	170 GeV	172.5 GeV	175 GeV
tb	$1.20^{+0.62}_{-0.56}$	$0.68^{+0.38}_{-0.35}$	$0.53^{+0.36}_{-0.34}$
SM	$1.12^{+0.04}_{-0.04}$	$1.04^{+0.04}_{-0.04}$	$0.98^{+0.04}_{-0.04}$
tqb	$2.65^{+0.65}_{-0.59}$	$2.86^{+0.69}_{-0.63}$	$2.45^{+0.60}_{-0.57}$
SM	$2.34^{+0.12}_{-0.12}$	$2.26^{+0.12}_{-0.12}$	$2.16^{+0.12}_{-0.12}$
$tb + tqb$	$3.70^{+0.78}_{-0.80}$	$3.43^{+0.73}_{-0.74}$	$2.56^{+0.69}_{-0.61}$
SM	$3.46^{+0.16}_{-0.16}$	$3.30^{+0.16}_{-0.16}$	$3.14^{+0.16}_{-0.16}$

C. tb, tqb and $tb + tqb$ channel cross sections

To measure the individual tb (tqb) production cross section, we construct a one-dimensional (1D) posterior probability density function with the tqb (tb) contribution normalized with a Gaussian prior centered on the predicted SM cross section and treated as a part of the background. This is implemented for each individual MVA method and also for their combination. To measure the total single top quark production cross section of $tb + tqb$, we construct a 1D posterior probability density function assuming the production ratio of tb and tqb predicted by the SM.

Figure 6 shows the expected and observed posterior density distributions for tb, tqb, and $tb + tqb$ using the combined discriminants B_{tb}, B_{tqb}, and B_{tb+tqb}, respectively. Table II lists the expected and measured cross sections for the individual MVA analyses. All of the results are consistent with SM predictions, and the measured $tb + tqb$ production cross section is the most precise current measurement, with a precision comparable to the world average [15]. All results assume a top quark mass of 172.5 GeV and have a small correction for events with more than four jets based on the SM. The dependence of the measured cross section on m_t is summarized in Table III. The assumed top quark mass affects the yield and differential properties for the signal acceptance and the modeling of $t\bar{t}$ events, which constitute the second largest background. The interplay between these two effects can cause the measured cross section to vary substantially (as observed in the tb channel) or in a way that is not monotonic with the assumed top quark mass (as observed in the tqb channel).

VI. SIGNAL DOMINATED DISTRIBUTIONS

Figure 7 shows a comparison of the distributions of four kinematic variables with large discriminating power, for single top quark production in a data sample selected with S:B >0.24 based on the B_{tb+tqb} discriminant. Variables shown are: leading b-tagged jets p_T, W boson transverse mass, centrality, defined as the ratio of the scalar sum of the

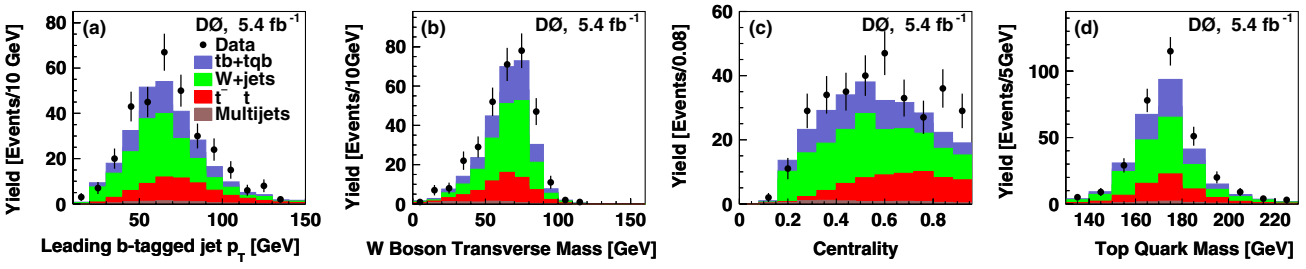

FIG. 7 (color online). [color online] Distributions for data in the regions of large value for signal discrimination: (a) leading b-tagged jet p_T, (b) W boson transverse mass, (c) centrality, defined as the ratio of the scalar sum of the p_T of the jets to the scalar sum of the energy of the jets in the event, and (d) reconstructed m_t. The contributions from signal have been normalized to the measured $tb + tqb$ cross section.

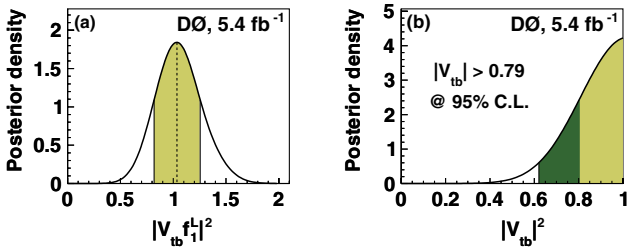

FIG. 8 (color online). The posterior density functions for (a) $|V_{tb}f_1^L|^2$ and (b) $|V_{tb}|^2$. The shaded (dark shaded) band indicates regions of 68% (95%) C.L. relative to the peak values.

p_T of the jets to the scalar sum of the energy of the jets in the event, and reconstructed m_t. The presence of the single top quark signal is needed to ensure a good description of the data.

VII. $|V_{tb}|$ MEASUREMENT

The single top quark production cross section is directly proportional to the square of the CKM matrix element $|V_{tb}|^2$, enabling us to measure $|V_{tb}|$ directly without any assumption on the number of quark families or the unitarity of the CKM matrix [17]. We assume that SM sources dominate for single top quark production and that top quarks decay exclusively to Wb. We also assume that the Wtb interaction is CP-conserving and of the $V-A$ type, but maintain the possibility for an anomalous strength of the left-handed Wtb coupling (f_1^L), which could rescale the single top quark cross section [48]. Therefore, we are measuring the strength of the $V-A$ coupling, i.e., $|V_{tb}f_1^L|$, which can be >1.

We form a Bayesian posterior $|V_{tb}f_1^L|^2$ with a flat prior based on the B_{tb+tqb} discriminant. Additional theoretical uncertainties are considered for the tb and tqb cross sections [2]. Using the measured $tb+tqb$ cross section, we obtain $|V_{tb}f_1^L| = 1.02^{+0.10}_{-0.11}$. If we restrict the prior to the SM region [0,1] and assume $f_1^L = 1$, we extract a limit of $|V_{tb}| > 0.79$ at the 95% C.L. Figure 8 shows the posterior density functions for $|V_{tb}f_1^L|^2$ and for $|V_{tb}|^2$, assuming $f_1^L = 1$ and $0 \leq |V_{tb}|^2 \leq 1$.

VIII. SUMMARY

In summary, we have measured the single top quark production cross section using 5.4 fb^{-1} of data collected by the D0 experiment at the Fermilab Tevatron Collider. For $m_t = 172.5$ GeV, we measure the cross sections for tb and tqb production to be

$$\sigma(p\bar{p} \to tb + X) = 0.68^{+0.38}_{-0.35}\ \text{pb}$$

$$\sigma(p\bar{p} \to tqb + X) = 2.86^{+0.69}_{-0.63}\ \text{pb}$$

assuming, respectively, tqb and tb production rates as predicted by the SM. These cross sections are consistent with the values measured in Ref. [30], where we use the same data set and discriminant but extract the tqb (tb) cross section without any assumption on the tb (tqb) production rate.

The total cross section $tb+tqb$ is found to be

$$\sigma(p\bar{p} \to tb + tqb + X) = 3.43^{+0.73}_{-0.74}\ \text{pb},$$

assuming the SM ratio between tb and tqb production. All measurements are consistent with the SM predictions for a top quark mass of 172.5 GeV. Finally, we derive a direct limit on the CKM matrix element $|V_{tb}| > 0.79$ at the 95% C.L. assuming a flat prior within $0 \leq |V_{tb}|^2 \leq 1$.

ACKNOWLEDGMENTS

We thank the staffs at Fermilab and collaborating institutions, and acknowledge support from the DOE and NSF (USA); CEA and CNRS/IN2P3 (France); FASI, Rosatom and RFBR (Russia); CNPq, FAPERJ, FAPESP and FUNDUNESP (Brazil); DAE and DST (India); Colciencias (Colombia); CONACyT (Mexico); KRF and KOSEF (Korea); CONICET and UBACyT (Argentina); FOM (The Netherlands); STFC and the Royal Society (United Kingdom); MSMT and GACR (Czech Republic); CRC Program and NSERC (Canada); BMBF and DFG (Germany); SFI (Ireland); The Swedish Research Council (Sweden); and CAS and CNSF (China).

[1] S. Moch and P. Uwer, Phys. Rev. D **78**, 034003 (2008). At $m_t = 172.5$ GeV, $\sigma(p\bar{p} \to t\bar{t} + X) = 7.46$ pb.
[2] N. Kidonakis, Phys. Rev. D **74**, 114012 (2006). The cross sections for the single top quark processes ($m_t = 172.5$ GeV) are 1.04 ± 0.04 pb (s channel), 2.26 ± 0.12 pb (t channel), and 0.28 ± 0.06 pb (tW channel).
[3] F. Abe *et al.* (CDF Collaboration), Phys. Rev. Lett. **74**, 2626 (1995).
[4] S. Abachi *et al.* (D0 Collaboration), Phys. Rev. Lett. **74**, 2632 (1995).
[5] T. Aaltonen *et al.* (CDF Collaboration), Phys. Rev. Lett. **103**, 092002 (2009).
[6] V. M. Abazov *et al.* (D0 Collaboration), Phys. Rev. Lett. **103**, 092001 (2009).
[7] S. Cortese and R. Petronzio, Phys. Lett. B **253**, 494 (1991).
[8] S. S. D. Willenbrock and D. A. Dicus, Phys. Rev. D **34**, 155 (1986).
[9] C.-P. Yuan, Phys. Rev. D **41**, 42 (1990).
[10] Unless otherwise stated, charge-conjugate states are implied.

[11] N. Cabibbo, Phys. Rev. Lett. **10**, 531 (1963); M. Kobayashi and T. Maskawa, Prog. Theor. Phys. **49**, 652 (1973).

[12] K. Nakamura *et al.* (Particle Data Group), J. Phys. G **37**, 075021 (2010).

[13] J. Alwall *et al.*, Eur. Phys. J. C **49**, 791 (2006).

[14] G. V. Jikia and S. R. Slabospitsky, Phys. Lett. B **295**, 136 (1992).

[15] The Tevatron Electroweak Working Group, for the CDF and D0 Collaborations. Report No. FERMILAB-TM-2440-E, 2009).

[16] V. M. Abazov *et al.* (D0 Collaboration), Phys. Rev. Lett. **98**, 181802 (2007).

[17] V. M. Abazov *et al.* (D0 Collaboration), Phys. Rev. D **78**, 012005 (2008).

[18] T. Aaltonen *et al.* (CDF Collaboration), Phys. Rev. Lett. **101**, 252001 (2008).

[19] T. Aaltonen *et al.* (CDF Collaboration), Phys. Rev. D **82**, 112005 (2010).

[20] S. Chatrchyan *et al.* (CMS Collaboration), Phys. Rev. Lett. **107**, 091802 (2011).

[21] T. Tait and C.-P. Yuan, Phys. Rev. D **63**, 014018 (2000).

[22] V. M. Abazov *et al.* (D0 Collaboration), Phys. Rev. Lett. **102**, 191802 (2009).

[23] V. M. Abazov *et al.* (D0 Collaboration), Phys. Lett. B **641**, 423 (2006); Phys. Rev. Lett. **100**, 211803 (2008); Phys. Lett. B **699**, 145 (2011).

[24] V. M. Abazov *et al.* (D0 Collaboration), Phys. Rev. Lett. **99**, 191802 (2007); Phys. Lett. B **693**, 81 (2010).

[25] A. P. Heinson, A. S. Belyaev, and E. E. Boos, Phys. Rev. D **56**, 3114 (1997).

[26] V. M. Abazov *et al.* (D0 Collaboration), Phys. Rev. Lett. **101**, 221801 (2008).

[27] V. M. Abazov *et al.* (D0 Collaboration), Phys. Rev. Lett. **102**, 092002 (2009).

[28] V. M. Abazov *et al.* (D0 Collaboration), Nucl. Instrum. Methods Phys. Res., Sect. A **565**, 463 (2006); Nucl. Instrum. Methods Phys. Res., Sect. A **584**, 75 (2008); Nucl. Instrum. Methods Phys. Res., Sect. A **622**, 298 (2010).

[29] V. M. Abazov *et al.* (D0 Collaboration), Phys. Lett. B **682**, 363 (2010).

[30] V. M. Abazov *et al.* (D0 Collaboration), arXiv:1105.2788 [Phys. Lett. B (to be published)].

[31] G. C. Blazey *et al.*, arXiv:hep-ex/0005012.

[32] V. M. Abazov *et al.* (D0 Collaboration), Nucl. Instrum. Methods Phys. Res., Sect. A **620**, 490 (2010).

[33] E. E. Boos *et al.*, Phys. At. Nucl. **69**, 1317 (2006). We use SINGLETOP version 4.2p1.

[34] Z. Sullivan, Phys. Rev. D **70**, 114012 (2004).

[35] J. M. Campbell, R. Frederix, F. Maltoni, and F. Tramontano, Phys. Rev. Lett. **102**, 182003 (2009).

[36] M. L. Mangano *et al.*, J. High Energy Phys. 07 (2003) 001. We use ALPGEN version 2.11.

[37] T. Sjöstrand, S. Mrenna, and P. Skands, J. High Energy Phys. 05 (2006) 026. We use PYTHIA version 6.409.

[38] R. Brun and F. Carminati, CERN Program Library Long Writeup, Report No. W5013, 1993.

[39] J. Alwall *et al.*, Eur. Phys. J. C **53**, 473 (2007); V. M. Abazov *et al.* (D0 Collaboration), Phys. Lett. B **669**, 278 (2008).

[40] R. K. Ellis, Nucl. Phys. B, Proc. Suppl. **160**, 170 (2006). We use MCFM version 5.1.

[41] I. M. Chakravarti, R. G. Laha, and J. Roy, *Handbook of Methods of Applied Statistics* (John Wiley and Sons, New York, 1967), Vol. I, pp. 370, 392–394.

[42] R. M. Neal, *Bayesian Learning for Neural Networks* (Springer-Verlag, New York, 1996).

[43] L. Breiman *et al.*, *Classification and Regression Trees* (Wadsworth, Stamford, 1984).

[44] K. O. Stanley and R. Miikkulainen, Evolutionary Computation **10**, 99 (2002).

[45] A variable is considered well-modeled if the mean Kolmogorov-Smirnov test [41] evaluated for the six analysis channels is greater than 0.3. For most variables, the value is greater than 0.5.

[46] A. Höcker, P. Speckmayer, J. Stelzer, J. Therhaag, E. von Toerne, and H. Voss, Proc. Sci., ACAT (2007) 040 [arXiv:physics/0703039].

[47] J. H. Friedman and B. E. Popescu, Ann. Appl. Stat. **2**, 916 (2008).

[48] G. L. Kane, G. A. Ladinsky, and C.-P. Yuan, Phys. Rev. D **45**, 124 (1992).

[49] The pseudorapidity is defined as $\eta = -\ln[\tan(\theta/2)]$, where θ is the polar angle relative to the proton beam direction.